MIDINET: Multi-Slice Inter-regional Distance-Based Individual Structural Brain Network

1st Xiaoye Bin#
Department of Artificial Intelligence
Nanjing University of Aeronautics and Astronautics
Nanjing, China
bin_xy@nuaa.edu.cn

2nd Chuang Liang#
Department of Artificial Intelligence
Nanjing University of Aeronautics and Astronautics
Nanjing, China
liangchuang@nuaa.edu.cn

3rd Tulay Adali
Department of CSEE
University of Maryland
Baltimore County, MD, USA
adali@umbc.edu

4th Vince D. Calhoun
Tri-institutional Center for Translational Research in Neuroimaging and Data Science (TReNDS)
Georgia State University, Georgia Institute of Technology, Emory University
Atlanta, GA, USA
vcalhoun@gsu.edu

5th Shile Qi*
Department of Artificial Intelligence
Nanjing University of Aeronautics and Astronautics
Nanjing, China
shile.qi@nuaa.edu.cn

***Abstract*—Unlike group-level networks, individualized structural brain networks are constructed based on region-to-region structural magnetic resonance imaging (sMRI) connectivity at individual-level to capture individual heterogeneity. However, most construction methods overlook the hierarchical distribution patterns of the brain, limiting their ability to capture subtle microstructural variations. To address this, we propose a novel framework: Multi-slice Inter-regional Distance-based Individual Structural Brain Network (MIDINet), which divides each brain region into anatomically ordered slices and extracts slice-wise multi-features to construct inter-regional similarity networks, thereby preserving spatial patterns and better capturing intra-regional heterogeneity. Results show that MIDINet generally outperforms the alternative approaches across diagnostic tasks and classifiers. The identified interpretable diagnostic biomarkers indicate that structural abnormalities associated with psychiatric disorders are more likely concentrated in higher-order cognition and emotion regions rather than in lower-level sensory or motor areas. In summary, MIDINet provides new insights into individualized structural brain networks and facilitates the precise diagnosis and mechanistic understanding of psychiatric disorders.**

Keywords—Individual structural brain network, slice-wise feature, psychiatric disorders, diagnostic biomarkers

I. INTRODUCTION

Brain network analysis has been extensively applied to investigate psychiatric disorders, offering a systems-level perspective that aligns with the "connectopathy" hypothesis in psychiatry. [1] Accumulating evidence links disorders such as schizophrenia (SZ) and autism spectrum disorder (ASD) to systematic disruptions in the topology of brain networks, including impaired structural integration and altered small-world properties [2-4]. Importantly, structural brain networks derived from structural magnetic resonance imaging (sMRI) offer a complementary perspective to functional networks by reflecting long-term neurodevelopmental and neuroanatomical constraints [5], which are less sensitive to transient cognitive or physiological states. However, most existing studies have been conducted on the group level and rely primarily on functional imaging, which overlooks inter-individual heterogeneity and is further constrained by long acquisition times [6], large data demands, and low test–retest reliability [7], thereby impeding precise characterization of structural abnormalities and subject-specific variations. There is increasing consensus that individualized brain network modeling is essential for precision psychiatry [8], where subject-specific biomarkers are required for accurate diagnosis, prognosis, and treatment stratification [9-11]. Hence, individualized structural brain network analysis is crucial for capturing subject-specific patterns and improving the accuracy and interpretability of psychiatric disorder diagnosis.

Current approaches for constructing individualized structural brain networks can be broadly categorized into three categories: correlation-based, divergence-based, and distance-based methods. Correlation-based methods estimate inter-regional similarity by directly correlating structural features across regions. Representative examples include voxel-based morphometry (VBM) [12], which compares whole-brain features at the voxel level, or alternatively averages parameter estimates (e.g., gray matter volume, GMV) within predefined ROIs to derive mean values for subsequent group-level statistical analyses. Cube-based segmentation has also been adopted to preserve neighborhood-level spatial continuity, yielding intermediate-scale representations suitable for graph-based learning [13]. While effective in capturing coarse inter-regional similarity, correlation-based methods often neglect fine-grained spatial variations within regions. Divergence-based methods instead quantify differences between feature distributions across regions. Kullback–Leibler (KL) [14] divergence has been applied to measure inter-regional GMV differences, providing a probabilistic perspective for individualized brain network construction. Jensen–Shannon (JS) divergence [15] has been employed to achieve a more symmetric and bounded comparison between regional feature

# These authors contributed equally to this work
* Corresponding author

This work was supported by the Key Research and Development Plan of Jiangsu Province, China (BE2023668), and the National Natural Science Foundation of China (62376124, 82371510). The authors declare no conflict of interests.

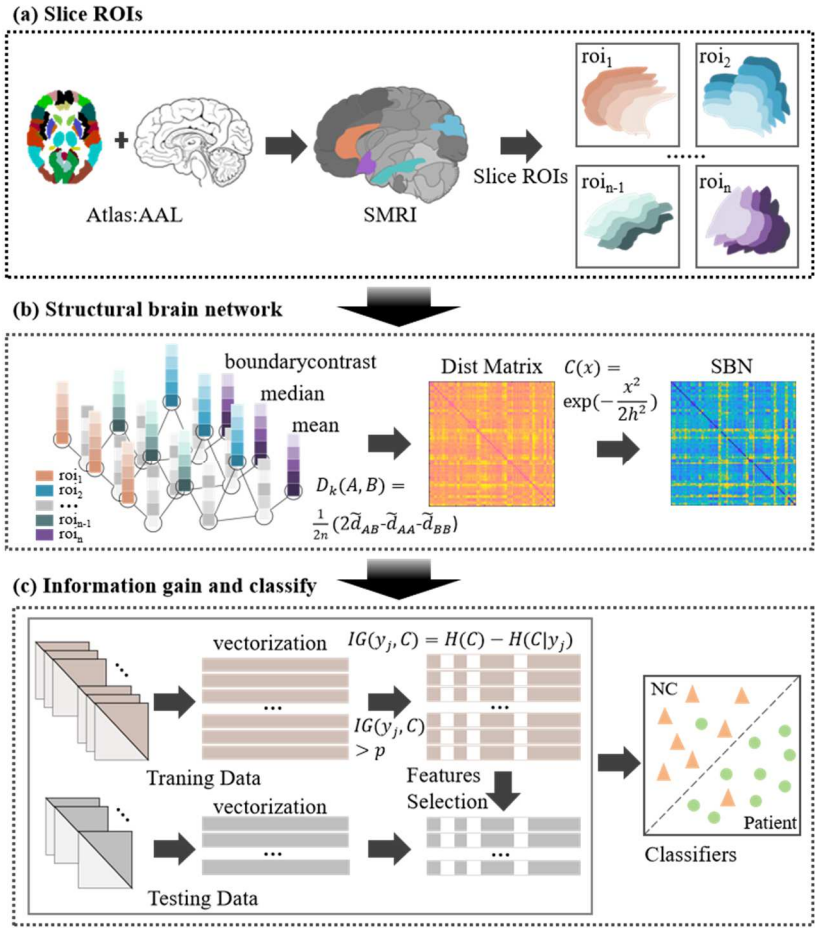

Fig. 1. Flowchart of the proposed MIDINet framework. (a) ROI parcellation and spatial slicing along the anatomical axis. (b) Slice-wise feature extraction for structural brain network construction. (c) Feature selection via information gain to reduce dimensionality for disease classification.

distributions. These approaches enhance sensitivity to distributional shifts but typically ignore spatial ordering between regions. Distance-based methods characterize structural similarity by computing distances between region-level feature representations [16]. Leming et al. employed the Earth Mover's Distance (EMD) to capture structural similarity patterns by leveraging the concept of "transport cost" between probability distributions to better detect atypical spatial configurations [17]. More recently, several individualized structural covariance network (SCN) [18] approaches have been proposed and used for psychiatric disorder diagnosis, including the reference-driven SCN (REF-SCN), the symmetric KL-divergence–based SCN (KLS-SCN), and individualized SCNs (iSCNs), which demonstrate improved diagnostic performance for schizophrenia and other psychiatric disorders [19-21]. Although effective in capturing inter-regional structural relationships through feature distribution comparisons, these methods typically treat voxel-level features within a region as unordered sets, thereby neglecting the hierarchical and directional distribution patterns that characterize brain tissue. This flattening of intra-regional spatial structure compromises the biological interpretability of the resulting brain networks and limits their ability to capture critical spatial variation patterns, particularly those underlying inter-individual heterogeneity.

To address these limitations, we propose a novel framework for constructing individualized structural brain networks, named Multi-Slice Inter-regional Distance-based Individual Structural Brain Network (MIDINet), designed to capture the hierarchical and directional morphological features within brain regions. Specifically, each ROI is segmented into contiguous two-dimensional slices aligned along its principal anatomical axis. Within each slice, three statistical features of local gray matter volume—mean intensity, median intensity, and boundary contrast—are extracted and assembled into a serialized representation that preserves anatomical ordering. Inter-regional similarity networks are then constructed by computing distances between multi-slice feature sequences of different regions. By leveraging multiple slice-level descriptors, this framework not only preserves the spatial distribution characteristics of gray matter but also captures intra-regional structural heterogeneity along the principal axis, thereby enhancing the robustness and interpretability of network-level structural representations.

II. Methods and Materials

The proposed framework focuses on individualized structural brain network construction and is designed to preserve intra-regional spatial organization while maintaining compatibility with a wide range of downstream classifiers. All methodological components are implemented in a subject-wise manner to avoid group-level information leakage.

A. Multi-slice division

To preserve the internal spatial laminar architecture of the brain, individual sMRI scans are preprocessed by SPM12 (Statistical Parametric Mapping, version 12), and 90 regions

TABLE I THE DIAGNOSTIC PERFORMANCE (%) ON THE ASD COMPARING MIDINET WITH OTHER ALTERNATIVE METHODS ACROSS 4 CLASSIFIERS

Classifiers	SVM		RF		GBDT		KNN	
Performance	ACC	AUC	ACC	AUC	ACC	AUC	ACC	AUC
cube	57.74±4.72	58.45±5.13	54.63±3.77	54.27±4.73	52.36±3.01	52.97±3.20	54.91±3.29	54.53±3.56
ROI-mean	56.34±3.79	56.36±3.92	56.32±3.18	56.04±3.47	57.28±3.22	56.93±3.52	57.11±3.86	56.79±4.17
KL	61.62±3.83	61.98±4.24	60.18±3.90	59.93±4.15	58.90±5.87	58.51±6.11	59.92±6.83	59.54±7.14
EMD	61.34±3.85	61.12±4.35	62.30±5.12	61.92±5.34	60.43±3.86	60.13±4.13	62.91±3.77	62.66±4.03
REF-SCN	55.99±5.95	58.09±6.27	63.44±4.33	66.63±5.38	58.94±3.73	61.58±4.79	57.77±2.74	60.92±6.26
KLS-SCN	59.93±3.98	63.26±2.93	66.68±4.32	66.34±3.88	63.26±3.65	65.14±6.01	61.82±6.16	65.27±6.93
iSCNs	65.95±2.37	68.62±4.00	61.91±3.66	63.74±5.76	64.96±1.96	64.38±4.50	61.91±2.36	62.11±4.96
MIDINet	**67.57±4.07**	**70.27±4.82**	**67.19±4.23**	**66.91±4.41**	**65.67±6.19**	**65.38±6.44**	**66.93±4.18**	**66.63±4.46**

TABLE II THE DIAGNOSTIC PERFORMANCE (%) ON THE SZ COMPARING MIDINET WITH OTHER ALTERNATIVE METHODS ACROSS 4 CLASSIFIERS.

Classifiers	SVM		RF		GBDT		KNN	
Performance	ACC	AUC	ACC	AUC	ACC	AUC	ACC	AUC
cube	65.69±8.68	65.26±8.97	67.80±3.58	67.81±3.41	66.34±5.27	66.28±5.33	67.32±3.33	67.21±3.40
ROI-mean	67.98±4.76	68.04±4.74	67.12±4.54	67.07±4.42	69.44±3.97	69.09±4.17	65.29±6.17	64.93±6.41
KL	72.82±9.15	72.51±9.43	73.84±3.51	73.52±3.74	70.98±3.96	70.76±4.43	70.20±3.55	70.33±3.52
EMD	75.08±4.79	75.11±4.72	75.91±5.37	75.60±5.63	74.55±4.65	74.52±4.74	71.49±3.22	71.36±3.10
REF-SCN	70.65±6.75	74.98±5.88	66.60±5.73	76.37±5.25	66.07±5.34	74.53±5.51	61.54±4.97	64.85±5.92
KLS-SCN	75.99±5.82	81.42±5.67	75.49±9.42	81.57±5.95	69.88±6.35	76.69±4.76	65.83±4.41	69.30±4.97
iSCNs	83.79±5.10	84.03±4.12	77.46±6.21	78.47±4.79	81.28±3.75	83.47±4.21	74.41±7.41	77.35±9.66
MIDINet	**85.76±3.28**	**85.42±3.45**	**84.57±5.03**	**84.26±5.25**	**84.61±3.19**	**84.34±3.33**	**85.37±5.26**	**85.14±5.40**

of interest (ROIs) are extracted according to the Automated Anatomical Labeling (AAL) [22], excluding cerebellar regions (**Fig. 1a**). For each ROI, gray matter voxels are extracted, and their spatial distribution is characterized using a covariance matrix C:

$$C = \frac{1}{N}\sum_{i=1}^{N}(X_i - \overline{X})(X_i - \overline{X})^T \quad (1)$$

where $X_i \in R^3$ denotes the three-dimensional coordinate of the i-th voxel, $\overline{X}$ is the centroid of the ROI, and N is the total number of voxels. Eigenvalue decomposition of C is performed as:

$$Cv_k = \lambda_k v_k, k = 1,2,3 \quad (2)$$

where the eigenvector v_k corresponding to the largest eigenvalue λ_k is defined as the principal axis of the region, with $k = 1,2,3$ denoting the three orthogonal eigenvectors of the covariance matrix. Distances along the principal axis are uniformly partitioned into n consecutive spatial slices to preserve anatomical ordering. This slice-wise partitioning allows the preservation of ordered spatial information along the dominant anatomical direction of each region. As a result, morphological variations across slices can be explicitly modeled rather than being collapsed into a single aggregated representation. In this study, the number of slices n is empirically determined based on preliminary experiments evaluating multiple candidate values, and $n = 45$ is selected as it achieved the most consistent performance across datasets. The same setting is then fixed and used in all subsequent experiments.

B. Construction of individual structural brain network

An individual structural connectivity network is constructed by extracting three types of GMV from each spatial slice (**Fig. 1b**): mean intensity (the average GMV within the slice), median intensity (the median GMV within the slice), and boundary contrast (the difference between the mean GMV of boundary voxels and that of interior voxels). For each brain region, these slice-level features are organized into a feature matrix $A \in R^{n\times 3}$, where each row corresponds to one slice and contains its three feature values, and n denotes the total number of slices. To quantify inter-regional structural similarity, a weighted multi-view feature distance $D_w(A,B)$ was defined between two brain regions A and B as follows:

$$D_w(A,B) = \frac{1}{n}\sum_{i=1}^{n}\sum_{j=1}^{n}\| a_i - b_j\|_w - \frac{1}{2n}\sum_{i=1}^{n}\sum_{j=1}^{n}(\|a_i - a_j\|_w + \|b_i - b_j\|_w) \quad (3)$$

where a_i and b_j represent the feature vectors of the i-th slice from brain regions A and B, respectively. The weighted distance metric $\|\cdot\|_w$ is defined as:

TABLE III ABLATION STUDY OF MIDINET ON SLICE-LEVEL FEATURES.

Features			ASD vs. NC		SZ vs. NC	
mean	**median**	**boundary contrast**	**ACC**	**AUC**	**ACC**	**AUC**
√			65.26±3.67	65.87±3.83	83.12±7.24	83.22±7.17
	√		63.84±4.16	63.54±4.34	81.35±6.88	81.04±6.61
		√	61.55±3.81	61.35±4.08	79.51±7.37	79.76±6.72
√	√		66.92±4.17	66.63±4.32	84.29±6.14	84.97±6.42
√		√	65.89±4.81	65.66±5.01	83.91±4.28	83.76±5.21
	√	√	65.47±5.14	65.28±5.39	82.17±4.96	82.65±5.59
√	**√**	**√**	**67.57±4.07**	**70.27±4.84**	**85.76±3.28**	**85.42±3.45**

$$\|x-y\|_w = \sqrt{\sum_{k=1}^{3}[w_k\,(x^{(k)}-y^{(k)})]^2}, \quad s.t.\sum_{k=1}^{3} w_k = 1, w_k \geq 0 \tag{4}$$

where $w = [w_1, w_2, w_3]^{\mathrm{T}}$ denotes the pre-assigned weights for the three feature types, which are empirically determined on the training set to balance their contributions, and then fixed and consistently applied to both the training and testing sets, This design enables different slice-wise morphological descriptors to contribute in a balanced manner to the inter-regional similarity measurement. The terms $x^{(k)}, y^{(k)}$ represent the k-th element of the feature vectors x and y, respectively.

After computing all pairwise distances, a symmetric distance matrix $D \in R^{m\times m}$ is obtained, where m is the number of brain regions. The distances are then transformed into connectivity strengths using a Gaussian kernel:

$$C_{ij} = \exp\left(-\frac{D_w(A_i, A_j)^2}{2h^2}\right), i, j = 1, \ldots, m \tag{5}$$

where C_{ij} is the connection strength between brain regions i and j, and A_i, A_j denote the feature matrices of regions i and j. The kernel bandwidth parameter h is set to the median of the off-diagonal elements in the distance matrix:

$$h = \mathrm{median}(\{D_{ij} | i < j\}) \tag{6}$$

C. Information gain module

To reduce feature redundancy in the network and enhance disease classification performance, feature vectors are extracted from the upper triangular elements of the connectivity matrix C, yielding $\mathrm{v} \in R^{m(m-1)/2}$. On the training set, information gain (IG) [23] is employed to identify discriminative connectivity features (**Fig. 1c**):

$$IG_k = H(y_{train}) - H(y_{train} \mid X_k) \tag{7}$$

$$H(Y) = -\sum_{c=1}^{C} p(c)\log_2 p(c) \tag{8}$$

where $H(Y)$ denotes the differential entropy, y_{train} represents the class labels in the training set, and X_k refers to the value vector of the k-th connectivity feature. The term $p(c)$ indicates the empirical probability of class c. A significance threshold $p = 0.01$ is adopted to retain features satisfying $IG_k > p$, which are subsequently applied to the test set for downstream classification analysis.

D. Datasets

Two independent datasets are used in this study. One is from the Autism Brain Imaging Data Exchange (ABIDE), including 521 ASDs (14.8 ± 9.0 years) and 592 age-gender matched normal controls (NCs, 15.0 ± 9.3 years) [24]. Another cohort, Bipolar and Schizophrenia Network for Intermediate Phenotypes (BSNIP), consisting of 177 SZs (34.6 ± 12.0 years) and 219 age-gender matched NCs (38.8 ± 12.6 years) [25]. sMRI data is available for each of these participants that are used in model training and testing. These two datasets differ substantially in age range, diagnostic categories, and imaging acquisition sites, providing a heterogeneous evaluation setting. Evaluating the proposed method across both datasets allows the assessment of its robustness and generalizability under varying demographic and clinical conditions. All analyses are performed in a subject-wise manner without mixing information across datasets.

III. RESULTS

A. The performance in diagnosing psychiatric disorders

We compare the diagnostic performance of the MIDINet with several advanced brain network construction methods, including Cube-based [13], ROI-mean [12], KL-divergence [14], and EMD [17]. The performance is assessed by computing the classification accuracy (ACC) and area under the ROC curve (AUC) under a 10-fold cross-validation. Furthermore, the robustness of MIDINet is validated on four widely used classifiers, including support vector machine (SVM), random forest (RF), gradient boosting decision tree (GBDT), and k-nearest neighbors (KNN). **Table I** and **Table II** present the diagnostic performance of ASD and SZ under different classification models, with the highest performance marked in bold. Results show that MIDINet generally outperforms the other alternative methods across four classifiers and two independent datasets, achieving the highest accuracy of 67.57% for ASD and 85.76% for SZ under the SVM classifier, thereby providing evidence for its

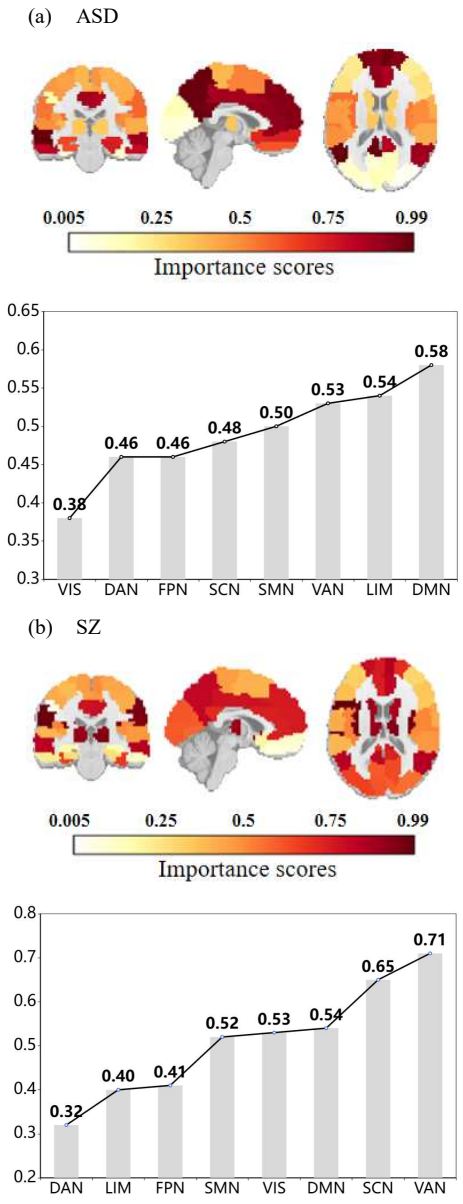

Fig. 2. The importance scores of individual brain regions for (a) ASD and (b) SZ diagnosis and the contribution order of the eight networks.

effectiveness. In addition, MIDINet achieves consistently superior performance across four classifiers, indicating that its extracted network features generalize well across different learning back-ends. This classifier-agnostic behavior reduces the likelihood that the improvements are driven by a particular model choice and suggests that the proposed structural representation captures stable and discriminative morphological patterns for distinguishing both ASD and SZ.

B. Feature ablation analysis

A series of ablation experiments are undertaken to validate the contributions of three slice-level feature types, including mean GMV, median GMV, and boundary contrast. Results are shown in Table III, with the highest performance marked in bold. Incorporating all three slice-level feature types within the MIDINet framework yields the optimal performance, indicating that multi-feature integration provides a more comprehensive structural representation than any single feature alone. Notably, each feature type contributes complementary information to classification, and removing any single component results in a noticeable performance drop, which confirms that the three descriptors capture non-redundant aspects of morphology. This observation supports our design choice of integrating multiple slice-level descriptors to better model complex and heterogeneous structural alterations, thereby improving the discriminability and robustness of the constructed individualized networks.

C. Biological interpretability

Occlusion sensitivity analysis [26, 27] is used to quantitatively assess the importance of each brain region to the classification process. Leveraging the correspondence between AAL and Yeo 7-network [28], all ROIs are divided into seven networks, including visual network (VIS), somatomotor network (SMN), dorsal attention network (DAN), ventral attention network (VAN), limbic network (LIM), frontoparietal control network (FPN), and default mode network (DMN), along with an additional subcortical network (SCN).

For each functional network, the importance score is calculated by aggregating the contributions of its constituent regions. The top three networks contributing the most to the diagnosis are DMN, LIM, and VAN for ASD, and VAN, SCN, and DMN for SZ (**Fig. 2**). These findings align with large-scale neuroimaging studies of psychiatric disorders, which have reported convergent structural and functional abnormalities in the DMN, LIM, SCN and VAN [29, 30]. Our results further indicate that structural abnormalities associated with ASD and SZ are predominantly concentrated in higher-order systems involved in cognitive integration and emotional regulation, rather than in lower-order sensory or motor regions.

IV. Conclusions

In summary, we proposed a novel individual-level structural brain network construction framework, MIDINet, to better capture the hierarchical and directional morphological features that may underlie inter-individual heterogeneity. Results showed that the proposed MIDINet framework achieved superior performance in the diagnostic tasks of psychiatric disorders and significantly outperformed alternative methods across four classifiers, underscoring its effectiveness and robustness. Feature ablation analysis demonstrated that combining mean GMV, median GMV, and boundary contrast at the slice level yields more robust representations than using any single feature alone. Beyond diagnostic performance, the proposed framework provides an interpretable [31] representation of individualized structural organization by explicitly modeling intra-regional spatial patterns. This characteristic makes MIDINet particularly suitable for applications that require both accuracy and neurobiological interpretability. The identified DMN, LIM, and VAN for ASD, as well as VAN, SCN, and DMN for SZ indicated that structural abnormalities associated with psychiatric disorders are more likely concentrated in higher-order brain regions involved in cognitive integration and emotional regulation rather than in lower-level sensory or motor areas. Overall, MIDINet provides a generalizable and interpretable framework that advances individualized structural brain network construction, offering novel opportunities for precision diagnosis and mechanistic understanding of psychiatric disorders.

References

[1] M. Rubinov and E. Bullmore, "Fledgling pathoconnectomics of psychiatric disorders," Trends Cogn. Sci., vol. 17, no. 12, pp. 641–647, 2013.

[2] Y. Xie et al., "Alterations in connectome dynamics in autism spectrum disorder: a harmonized mega-and meta-analysis study using the autism brain imaging data exchange dataset," Biological psychiatry, vol. 91, no. 11, Month, pp. 945-955, 2022.

[3] B. Lu et al., "Same same but different: Neuroanatomic and connectomic profiles of early-onset schizophrenia and autism spectrum disorder," Medicine Plus, vol. 1, no. 1, Month, pp. 100007, 2024.

[4] S. J. Abplanalp, D. L. Braff, G. A. Light, K. H. Nuechterlein, M. F. Green, and S. Consortium on the Genetics of, "Understanding Connections and Boundaries Between Positive Symptoms, Negative Symptoms, and Role Functioning Among Individuals With Schizophrenia: A Network Psychometric Approach," JAMA Psychiatry, vol. 79, no. 10, Month, pp. 1014-1022, 2022.

[5] Z. Guo et al., "Systematic review and meta-analysis: multimodal functional and anatomical neural alterations in autism spectrum disorder," Molecular autism, vol. 15, no. 1, Month, pp. 16, 2024.

[6] I. Sungur et al., "Neuroanatomical subtyping for schizophrenia with machine learning," Psychiatry Res. Neuroimaging, vol. 353, p. 112058, 2025.

[7] C. Marzi, M. Giannelli, A. Barucci, C. Tessa, M. Mascalchi, and S. Diciotti, "Efficacy of MRI data harmonization in the age of machine learning: a multicenter study across 36 datasets," Scientific Data, vol. 11, no. 1, Month, pp. 115, 2024.

[8] M. K. K. Rony et al., "Artificial intelligence in psychiatry: A systematic review and meta-analysis of diagnostic and therapeutic efficacy," Digital Health, vol. 11, pp. 20552076251330528, 2025.

[9] M. Gell, S. Noble, T. O. Laumann, S. M. Nelson, and B. Tervo-Clemmens, "Psychiatric neuroimaging designs for individualised, cohort, and population studies," Neuropsychopharmacology, vol. 50, no. 1, Month, pp. 29-36, 2025.

[10] N. García-San-Martín et al., "Reduced brain structural similarity is associated with maturation, neurobiological features, and clinical status in schizophrenia," Nature Communications, vol. 16, no. 1, Month, pp. 8745, 2025.

[11] L. M. Williams and S. Whitfield Gabrieli, "Neuroimaging for precision medicine in psychiatry," Neuropsychopharmacology, vol. 50, no. 1, Month, pp. 246-257, 2025.

[12] J. Ashburner and K. J. Friston, "Voxel-based morphometry--the methods," Neuroimage, vol. 11, no. 6 Pt 1, Month, pp. 805-21, 2000.

[13] M. Cai et al., "Individual - level brain morphological similarity networks: current methodologies and applications," CNS neuroscience & therapeutics, vol. 29, no. 12, Month, pp. 3713-3724, 2023.

[14] S. Kullback and R. A. Leibler, "On information and sufficiency," The annals of mathematical statistics, vol. 22, no. 1, Month, pp. 79-86, 1951.

[15] J. Lin, "Divergence measures based on the Shannon entropy," IEEE Transactions on Information theory, vol. 37, no. 1, Month, pp. 145-151, 2002.

[16] L. Lin et al., "Voxel-based texture similarity networks reveal individual variability and correlate with biological ontologies," NeuroImage, vol. 297, pp. 120688, 2024.

[17] J. Wang and Y. He, "Toward individualized connectomes of brain morphology," Trends in Neurosciences, vol. 47, no. 2, Month, pp. 106-119, 2024.

[18] X. Shao et al., "Intra-individual structural covariance network in schizophrenia patients with persistent auditory hallucinations," Schizophrenia, vol. 10, no. 1, Month, pp. 92, 2024.

[19] C. S. Vetter et al., "Exploring the predictive value of structural covariance networks for the diagnosis of schizophrenia," Front Psychiatry, vol. 16, pp. 1570797, 2025.

[20] X. Kang et al., "Structural MRI-based Computer-aided Diagnosis Models for Alzheimer Disease: Insights into Misclassifications and Diagnostic Limitations," Radiol Artif Intell, vol. 7, no. 6, Month, pp. e240508, 2025.

[21] G.-J. Ji et al., "Linking personalized brain atrophy to schizophrenia network and treatment response," Schizophrenia Bulletin, vol. 49, no. 1, Month, pp. 43-52, 2023.

[22] N. Tzourio-Mazoyer et al., "Automated anatomical labeling of activations in SPM using a macroscopic anatomical parcellation of the MNI MRI single-subject brain," Neuroimage, vol. 15, no. 1, Month, pp. 273-89, 2002.

[23] K. Qu, J. Xu, Q. Hou, K. Qu, and Y. Sun, "Feature selection using Information Gain and decision information in neighborhood decision system," Applied Soft Computing, vol. 136, pp. 110100, 2023.

[24] A. Di Martino et al., "Enhancing studies of the connectome in autism using the autism brain imaging data exchange II," Sci Data, vol. 4, pp. 170010, 2017.

[25] C. A. Tamminga et al., "Clinical phenotypes of psychosis in the Bipolar-Schizophrenia Network on Intermediate Phenotypes (B-SNIP)," American Journal of psychiatry, vol. 170, no. 11, Month, pp. 1263-1274, 2013.

[26] P. H. Valois, K. Niinuma, and K. Fukui, "Occlusion sensitivity analysis with augmentation subspace perturbation in deep feature space," in 2024, pp. 4829-4838.

[27] M. D. Zeiler and R. Fergus, "Visualizing and understanding convolutional networks," in 2014, pp. 818-833.

[28] B. T. Yeo et al., "The organization of the human cerebral cortex estimated by intrinsic functional connectivity," J Neurophysiol, vol. 106, no. 3, Month, pp. 1125-65, 2011.

[29] Y. Du et al., "Evidence of shared and distinct functional and structural brain signatures in schizophrenia and autism spectrum disorder," Commun Biol, vol. 4, no. 1, Month, pp. 1073, 2021.

[30] M. C. Postema et al., "Altered structural brain asymmetry in autism spectrum disorder in a study of 54 datasets," Nat Commun, vol. 10, no. 1, Month, pp. 4958, 2019.

[31] E. H. Houssein, A. M. Gamal, E. M. Younis, and E. Mohamed, "Explainable artificial intelligence for medical imaging systems using deep learning: a comprehensive review," Cluster Computing, vol. 28, no. 7, Month, pp. 469, 2025.